Tectonic development of the southern Chinese Altai Range as determined by structural geology, thermobarometry, ^{40}Ar/^{39}Ar thermochronology, and Th/Pb ion-microprobe monazite geochronology

Stephanie M. Briggs[1,5,†], **An Yin**[1,2,3], **Craig E. Manning**[1], **Zheng-Le Chen**[3], **Xiao-Feng Wang**[3]

[1]*Department of Earth and Space Sciences, University of California, Los Angeles, California 90095, USA*
[2]*Institute of Geophysics and Planetary Physics, University of California, Los Angeles, California 90095, USA*
[3]*Structural Geology Group, School of Earth Sciences and Resources, China University of Geosciences, Beijing 100083, China*
[4]*Institute of Geomechanics, Chinese Academy of Geological Sciences, Beijing 100081, People's Republic of China*
[5]*William Lettis and Associates, Augusta, Georgia 30901, USA*

ABSTRACT

The 2500-km Altai Range is located in the central part of the Central Asia Orogenic System, a tectonic collage comprising oceanic and continental fragments that were assembled during the Paleozoic continental growth of Eurasia. We conducted field mapping, ^{40}Ar/^{39}Ar thermochronology, metamorphic petrology, and Th/Pb ion-microprobe monazite dating in the southern Chinese Altai Range. This study demonstrates the presence of a south-vergent, Permo-Triassic thrust belt active across the region. Metamorphic conditions of 610 ± 35 °C and 5.7 ± 1.8 kbar were reached by schists with Permo-Triassic monazite ages. Mica ^{40}Ar/^{39}Ar ages range from Late Permian to Jurassic, and cooling in these rocks is correlated with thrust faulting. This shortening was synchronous with localized left-lateral, strike-slip shear deformation. Our work suggests that the high-grade schists of the Altai orogen were buried to depths of more than 18–20 km and were exhumed in the Permian to Jurassic. The Permo-Triassic Altai thrust belt was reactivated locally by Late Jurassic contraction after ca. 160 Ma, which may result from the final closure of the Mongol-Okhotsk Ocean or the collision of the Lhasa block onto the southern Asian margin.

INTRODUCTION

The Central Asia Orogenic System is one of the largest Phanerozoic orogenic belts in the world (Fig. 1). It consists of oceanic and continental fragments assembled during the Paleozoic continental growth of Asia (Zonen-
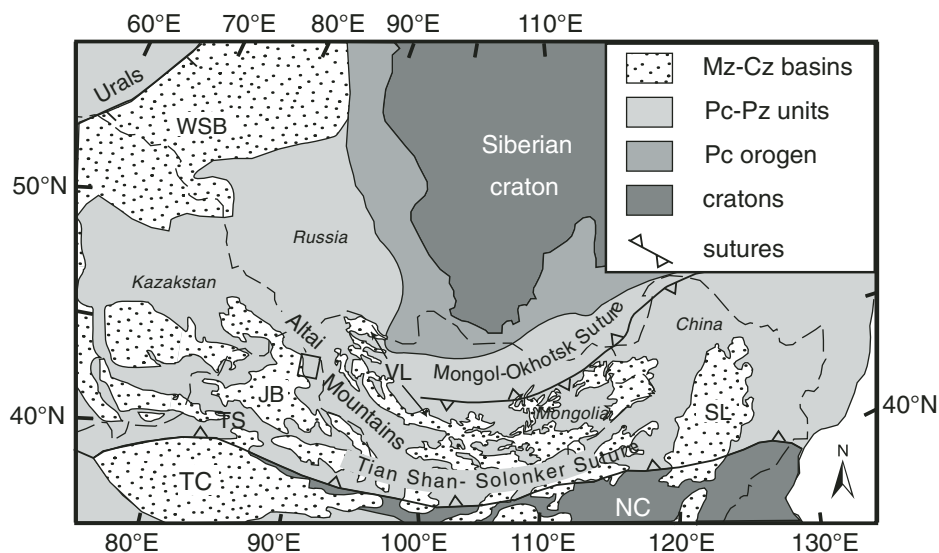
†E-mail: briggs@lettis.com

Figure 1. Generalized tectonic map of central Asia. Solid box is location of field area for this study. Abbreviations: TC—Tarim craton; JB—Junggar basin; NC—North China craton; SL—Songliao basin; VL—Valley of the lakes; WSB—West Siberian basin.

shain et al., 1990; Şengör et al., 1993; Şengör and Natal'in, 1996; Hsü and Chen, 1999; Chen and Jahn, 2002; Buslov et al., 2004; Jahn, 2004). Despite its importance in understanding the geologic history of Eurasia, exactly how the orogen was constructed remains highly uncertain (see a recent review by Windley et al., 2007, and references therein). Two contrasting mechanisms for Central Asia Orogenic System growth have emerged, with the first emphasizing collision of multiple arcs (Zonenshain et al., 1990; Dobretsov et al., 1995; Zorin, 1999; Badarch et al., 2002; Xiao et al., 2004; Briggs et al., 2007; Windley et al., 2007) and the second requiring duplication of a single, long-lived arc by synsubduction strike-slip faulting (Şengör et al., 1993; Allen et al., 1995; Şengör

and Natal'in, 1996). The above models make specific predictions on the timing and style of deformation across central Asia. For example, the multiple-arc–collision models emphasize the role of thrusting during oceanic subduction and subsequent ocean closure while the single-arc–duplication model requires coeval intra-arc strike-slip faulting and arc magmatism.

To test the above models for the Central Asia Orogenic System evolution, we conducted an integrated field, petrological, and geochronologic investigation across the southern Chinese Altai Range. The main purpose of this study is to determine the age and sense of motion of major structures and their relationships to regional arc magmatism and tectonic development of the Central Asia Orogenic System.

REGIONAL GEOLOGY

The northwest-trending Altai Range in central Asia extends ~2500 km, crossing China, Russia, Mongolia, and Kazakhstan (Fig. 1). The range has a crustal thickness of ~55 km (Wang et al., 2003) and is dominated by Cenozoic right-lateral, strike-slip transpressional tectonics (Tapponnier and Molnar, 1979; Cunningham et al., 1996a, 1996b; Cunningham, 2005). Cenozoic deformation initiated in the Eocene in the Russian Altai Range and progressively propagated southward to the southern Chinese Altai Range, where the deformation began in the Miocene (De Grave and Van den haute, 2002; De Grave et al., 2007; Yuan et al., 2006).

The Mesozoic history of the Altai Range remains poorly understood, and its relationship to the wide variety of deformation (from transpression to contraction to extension) reported during this time in adjacent regions in North China, Mongolia, and southern Siberia is uncertain (Lamb et al., 1999; Webb et al., 1999; Dumitru and Hendrix, 2001; Graham et al., 2001; Johnson et al., 2001; Sjostrom et al., 2001; Davis et al., 2002; De Grave and Van den haute, 2002; De Grave et al., 2007).

The dominant tectonic event in the Altai Range occurred during the creation and subsequent destruction of the Paleo-Asian Ocean from the Late Proterozoic to the Permian, a process leading to the ultimate formation of the Central Asia Orogenic System (Zonenshain et al., 1990; Şengör et al., 1993; Şengör and Natal'in, 1996; Windley et al., 2007). The orogenic event is manifested by the deformation of Neoproterozoic to Early Permian marine strata (dominantly arc-related turbidite and submarine volcanic sequences) and widespread occurrence of Paleozoic plutons (Zonenshain et al., 1990; Şengör et al., 1993; Badarch et al., 2002; Buslov et al., 2004; Windley et al., 2007). The ages of the Paleozoic plutons in the Chinese Altai Range are clustered at 470–377 Ma and 344–280 Ma, respectively (Han et al., 1997; Chen and Jahn, 2002; Windley et al., 2002; Wang et al., 2006; Briggs, 2007; Briggs et al., 2007). The early phase was calc-alkaline, whereas the second was alkali and aluminous (Mei et al., 1993; Han et al., 1997; Chen and Jahn, 2002; Xu et al., 2002; Wang et al., 2006).

STRUCTURAL GEOLOGY AND LITHOLOGY OF THE FUYUN AREA, SOUTHERN CHINESE ALTAI RANGE

The central location of the Altai Range in the Central Asia Orogenic System makes it an ideal place to test the existing tectonic models (e.g., Qu and Zhang, 1994; Travin et al., 2001; Windley et al., 2002; Laurent-Charvet et al., 2003; Buslov et al., 2004; Wang et al., 2006; Briggs, 2007; Briggs et al., 2007; Windley et al., 2007). Early geologic mapping in the Chinese Altai Range emphasized lithologic distributions (Xinjiang Bureau of Geology and Mineral Resources [BGMR], 1993), whereas our field investigation focused on the tectonic origin of lithologic assemblages, fault geometry, deformation kinematics, and temporal relationships among major structures. Our study area in the southern Chinese Altai Range is dominated by northwest-trending structures including foliation, distribution of mappable units, and a series of northwest-striking thrusts, folds, and ductile strike-slip shear zones. The active Fuyun right-lateral, strike-slip fault truncates all the northwest-trending structures (Fig. 2).

Thrusts

The southernmost major thrust in the Fuyun area is the Sarbulak fault (Fig. 2), which places Devonian volcanic rocks over Carboniferous graywacke and volcanic strata. Both hanging-wall and footwall units display axial cleavage associated with folding. The hanging wall is also imbricated by a north-dipping thrust zone that merges with the Ertix fault in the north and the Sarbulak thrust in the south (Fig. 2). This map relationship suggests that the imbricate thrusts are parts of a duplex system, with the Ertix thrust as the roof fault and the Sarbulak thrust as the floor thrust.

The Ertix thrust is northwest-striking in the western portion of the study area and east-striking in the eastern portion of the study area (Fig. 2). It juxtaposes an upper-amphibolite–facies gneiss complex over a chlorite-grade Devonian volcaniclastic sequence. The complex consists of quartzofeldspathic gneiss, metabasite, cherts, and deformed Ordovician–Silurian arc-related granitoids (470–400 Ma) that intrude into the above units (Wang et al., 2006; Briggs et al., 2007). The presence of metachert in the complex led Briggs et al. (2007) to interpret it as a deeply buried subduction mélange complex that was later exhumed by thrusting. This interpretation implies that the Ordovician arc was built upon a mélange complex.

The metamorphic rocks in the Ertix hanging wall were previously assigned a Precambrian age (e.g., Xinjiang BGMR, 1993; Windley et al., 2002). However, recent dating of the orthogneiss component in the complex yielded demonstrably igneous ages of ca. 450 Ma, which may be part of a Late Ordovician arc pluton brought up the surface by motion along the Ertix fault in the Permian (Briggs et al., 2007). Şengör et al. (1993) and Şengör and Natal'in

(1996) suggested that the Ertix fault was a major right-lateral structure with over 1600 km of offset in the Early Paleozoic at 520–340 Ma (Şengör et al., 1993; Şengör and Natal'in, 1996). However, kinematic studies of the fault zone, the contrast of metamorphic grade across the fault, and the presence of an inverted metamorphic zone in the hanging wall all suggest the fault is a thrust (Yang et al., 1992; Zhang et al., 1992; Qu and Zhang, 1994; O'Hara et al., 1997; Briggs et al., 2007). Th/Pb ion-microprobe dating of synkinematic monazite and a pressure-temperature (P-T) study of its hanging-wall rocks suggest that the fault was active in the Late Permian and exhumed amphibolite-grade rocks from >25 km to the shallow crustal levels (Briggs et al., 2007).
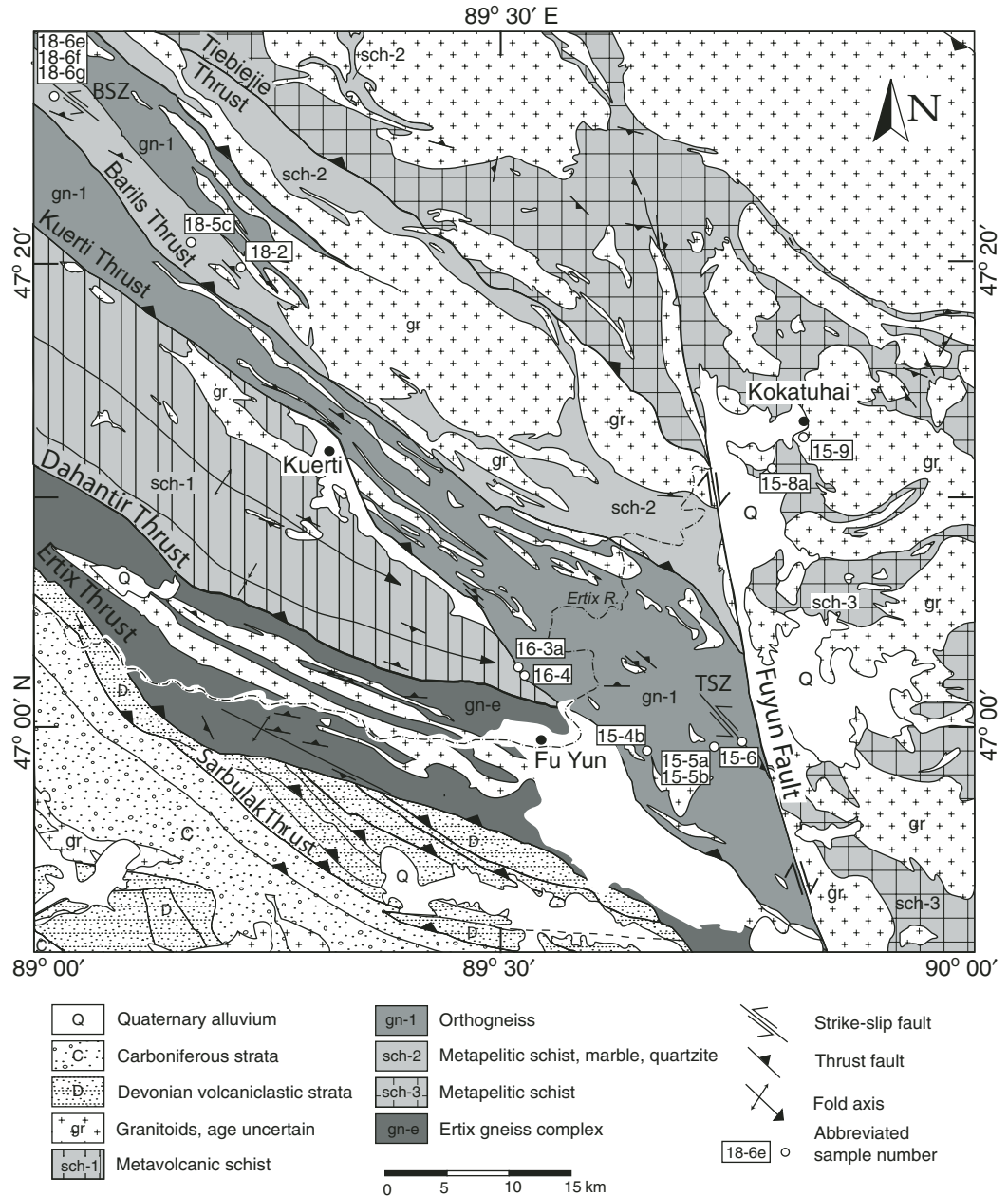
The Dahantir thrust is structurally above the Ertix thrust. It places a metavolcanic complex over the Ertix hanging wall. The hanging-wall rocks consist of mafic schist, metachert, metagraywacke and minor metagabbro (Xinjiang BGMR, 1993; Xu et al., 2002). From the interlayered radiolarian chert, Xu et al. (2002) assigned a Late Devonian–Early Carboniferous age for the metabasite complex. They further suggested these rocks represent portions of a backarc basin (also see Wang et al., 2006), while Windley et al. (2002) suggested they represent a forearc basin.

The trace of the Dahantir fault is parallel to the Ertix fault to the south in a nearly east-west direction but discordant to the NW-striking Kuerti thrust to the north (Fig. 2). The Dahantir hanging-wall units are penetratively foliated, with the foliation tightly folded into a pair of ESE-plunging antiform and synform (Fig. 2). The Dahantir fault and its hanging-wall folds are both truncated by the northwest-striking Kuerti fault at their eastern ends (Fig. 2), suggesting that the Danhantir fault is older than the Kuerti fault (i.e., the Kuerti fault is an out-of-sequence structure).

The Kuerti thrust generally strikes NW and dips to the northeast. When tracing the fault in the field, we found that the fault is warped, as indicated by rapid changes in fault attitude over short distances (tens of meters). The fault zone is defined by a cataclastic zone ~10 m wide with dominantly downdip striations. Cleavage is well developed in the fault gouge zone; its oblique angle to the fault surface indicates a top-south sense of thrusting.

The hanging wall of the Kuerti thrust is composed of orthogneiss with minor migmatite and peltic schists. The felsic orthogneiss consists of K-feldspar, plagioclase, quartz, amphibole, and biotite. The gneisses in the hanging wall have been assigned as Precambrian basement (e.g., Xinjiang BGMR, 1978, 1993; He et al., 1990),

Figure 2. Map of the Fuyun area in the southern Chinese Altai Range, based on a compilation of maps by Xinjiang Bureau of Geology and Mineral Resources (BGMR) (1978, 1993) and our own field observations. Sample sites (small white dots) are accompanied by abbreviated sample labels (e.g., 6.18.02.5c = 18-5c). Labels for strike-slip shear zones are also abbreviated: Balaerqishi Shear Zone—BSZ; Tuhongshat Shear Zone—TSZ.

Quaternary alluvium — Q
Carboniferous strata — C
Devonian volcaniclastic strata — D
Granitoids, age uncertain — gr
Metavolcanic schist — sch-1
Orthogneiss — gn-1
Metapelitic schist, marble, quartzite — sch-2
Metapelitic schist — sch-3
Ertix gneiss complex — gn-e
Strike-slip fault
Thrust fault
Fold axis
Abbreviated sample number — 18-6e

but no detailed geochronologic work has confirmed this speculation.

Discrete, thrust-type shear zones are present locally above the Kuerti thrust and display stretching mineral lineation trending ~N10°E and plunging 40°–50°. Minor folds are also present in the Kuerti hanging wall, with the hinges trending in the N60°W direction and plunging gently to the southeast at ~20°. These kinematic indicators are compatible with thrust kinematics, and the cataclasis at the trace of the fault could be interpreted as the final stage of deformation on this thrust, or a more recent reactivation.

The Barils thrust juxtaposes a metasedimentary sequence including schist, marbles, and quartzite (unit sch-2 in Fig. 2) over the Kuerti hanging wall described above. The metasediments were assigned an Ordovician–Silurian age based on regional lithologic correlations by Xinjiang BGMR (1978, 1993). Foliations in the schist unit have an average strike of ~N60°W and dip steeply between 76°NE to nearly vertical. Overlying the schist unit is a quartzofeldspathic gneiss unit, which is thrust over by the Tiebiejie thrust carrying a metasedimentary schist unit in its hanging wall (Fig. 2).

Ductile Strike-Slip Shear Zones

Zhang et al. (1992) documented the left-slip Tuehongshat shear zone (also known as the Erqishi shear zone of Laurent-Charvet et al. [2002, 2003]) in the Kuerti hanging wall. Laurent-Charvet et al. (2002, 2003) interpreted the shear zones to have moved in the Permo-Triassic (290–245 Ma) based on ^{40}Ar/^{39}Ar biotite and amphibolite ages. As shown below, this range of cooling ages is not unique to the strike-slip shear zones but rather is documented regionally throughout the entire southern Chinese Altai Range. This shear zone displays a

well-developed foliation with an average orientation of N47°W, 72°NE, and a mineral-stretching lineation that plunges gently (25°) to S53°E. Mapping indicates this shear zone is restricted in width (<100 m) and does not significantly offset units; hence we consider this to be a localized feature.

The left-slip Balaerqishi shear zone, location 6.18.02.6 in Figure 2, exhibits a nearly vertical attitude in the field, with the shear zone 80–100 m wide and striking N65°W. The shear zone is composed of highly stretched marble layers. Kinematic indicators such as asymmetric boudinage and rotated clasts show left-lateral sense of shear. The relationship between the strike-slip shear zone and the nearby Barils thrust is not clear, although the limited extent of the shear zone indicates it is a localized feature.

Cenozoic Structures

Active northwest-striking right-slip faulting currently dominates the Altai Range (Tapponnier and Molnar, 1979; Baljinnyam et al., 1993; Lin, 1994; Cunningham et al., 1996a, 1996b; Cunningham, 1998, 2001, 2005), whereas east-trending folds are present in the Cenozoic Junggar basin directly south of the range (Xinjiang BGMR, 1993). Because they are generally parallel, some of the active northwest-striking faults may be reactivated Paleozoic structures (e.g., Allen and Vincent, 1997).

The most prominent Cenozoic structure in the study area is the active right-slip Fuyun fault that cuts across all the northwest-striking structures described above (Fig. 2). Estimated

fault offset on the fault ranges from 8 to 20 km (Lin, 1994; Windley et al., 2002). To the north, the fault terminates into a northwest-trending, active right-slip fault zone in the Mongol Altai Range (Cunningham, 2005), where to the south it makes an abrupt turn to the east to become a northeast-dipping thrust (Laurent-Charvet et al., 2002, 2003).

PETROLOGY, ^{40}Ar/^{39}Ar THERMOCHRONOLOGY, AND TH/PB ION-MICROPROBE GEOCHRONOLOGY

In order to determine the pressure (P), temperature (T), and time (t) evolution associated with faulting across the Fuyun region of the Chinese Altai Range, we calculated P and T for mineral assemblages from metamorphic rocks, and performed Th/Pb ion-microprobe dating of monazite and ^{40}Ar/^{39}Ar thermochronology. Below, we describe the analytical methods used for this study followed by presentation of the results in the context of the structural framework described in the previous section.

Methods

Metamorphic Petrology

We used the University of California, Los Angeles (UCLA) JEOL JXA-8200 electron microprobe to make X-ray composition maps of garnets, determine their zoning patterns, and measure mineral compositions. An accelerating voltage of 15 kV and a current of ~100 nA were used for X-ray maps collected with 2 μm pixels

with a dwell time of 60 ms per pixel. For individual mineral analyses, a current of 10 nA was used with a beam focused to <1 μm diameter for all phases except plagioclase and micas, for which a spot diameter of 4–7 μm was used. Using X-ray maps or line traverses across garnets, we assessed garnet compositional trends. After making multiple measurements of each matrix phase to ensure for consistency, those results were paired with garnet analyses with the lowest Fe# (Fe/(Fe + Mg)) values. Intersections of garnet-biotite and garnet-biotite-muscovite-plagioclase equilibria were calculated using A-X and THERMOCALC (Holland and Powell, 1998). Table 1 presents the representative mineral analyses and resulting P-T conditions for each sample.

Th-Pb Monazite Dating

We investigated the age of metamorphism and its relationship to deformation using in situ Th-Pb dating of monazite. This method allows direct examination of the textural relationships between monazite grains and metamorphic or tectonic fabrics (Harrison et al., 1995). Monazite, often very small (<15 μm in diameter), appears bright when using the scanning electron microscope (SEM) in backscatter mode. Once identified, we used the ion microprobe to date grains in situ following procedures of Catlos et al. (2002). The UCLA CAMECA IMS-1270 secondary ion microprobe was used with a beam current of 10 to 15 nA focused to a size of 15–30 μm in diameter. Monazite standard 554 (45 ± 1 Ma; Harrison et al., 1999) was used.

TABLE 1. REPRESENTATIVE ELECTRON MICROPROBE ANALYSES AND THERMOBAROMETRY RESULTS

Phase	TiO$_2$	SiO$_2$	Na$_2$O	FeO*	K$_2$O	Cr$_2$O$_3$	Al$_2$O$_3$	MgO	MnO	CaO	Total	P and T
Sample 6.18.02.2: Grt Bt Ms Pl Q												
Muscovite	0.458	46.23	1.056	2.328	8.248	0	36.152	0.638	0	0.02	95.13	**P**
Biotite	1.808	36.588	0.255	19.321	7.935	0.12	19.789	10.113	0.14	0.034	96.103	**5.8 ± 1.7**
Plagioclase	0†	56.886	7.247	0.098	0.05	0.063	25.728	0.023	0	6.99	97.085	**T**
Garnet	0.064	36.656	0.02	27.611	0.005	0.097	21.598	2.783	9.39	2.456	100.68	**643 ± 141**
Sample 6.18.02.5c: Grt Bt Ms Pl Q												
Biotite	2.188	36.305	0.197	19.274	9.14	0.025	20.197	11.139	0.184	0.098	98.75	**P**
Garnet	0.055	36.702	0.01	32.335	0.015	0	21.574	3.135	6.451	0.664	100.94	**5.3 ± 1.9**
Muscovite	0.547	47	1.183	1.074	9.813	0	37.983	0.692	0	0.003	98.30	**T**
Plagioclase	0	64.405	10.517	0.019	0.04	0	21.546	0	0.014	2.245	98.79	**565 ± 117**
Sample 6.18.02.6e: Grt Bt St Ms Pl Q												
Staurolite	0.047	26.101	0.023	0.33	0.006	0.443	54.758	1.739	13.712	0	97.16	**P**
Garnet	0.067	36.222	0	4.951	0	0	21.524	2.777	32.903	0.817	99.26	**7.0 ± 2.0**
Muscovite	0.043	43.925	1.44	0	8.579	0.65	34.423	0.709	1.438	0.012	91.22	**T**
Plagioclase	0.027	63.464	10.004	0.005	0.033	0	22.399	0.02	0.203	3.164	99.32	**664 ± 70**
Biotite	0.018	35.46	0.228	0.086	8.365	1.654	19.582	10	17.536	0.059	92.99	
Sample 6.18.02.6f: Grt Bt Ms St Pl Q												
Biotite	1.465	35.137	0.278	17.473	8.4	0.058	19.505	10.694	0.062	0	93.07	**P**
Muscovite	0.613	44.335	1.506	1.036	8.434	0.079	35.166	0.497	0.012	0	91.68	**5.0 ± 1.8**
Plagioclase	0.019	62.974	9.791	0.055	0.044	0	22.21	0	0.03	3.234	98.36	**T**
Garnet	0.063	36.666	0.026	31.74	0.023	0.025	21.301	2.992	4.961	1.121	98.92	**590 ± 40**

Note: Average P-T calculations from THERMOCALC version 3.1 with May 2001 database (Holland and Powell, 1998). Mineral formulas and activities were calculated with the program A-X by Tim Holland and Roger Powell. Uncertainties are listed at the 95% confidence level. Abbreviations: Bt—biotite; Grt—garnet; Ms—muscovite ; P—pressure; Pl—plagioclase; Q—quartz; St—staurolite; T—temperature.
  *All iron as FeO.
  †0 is not detected.

$^{40}Ar/^{39}Ar$ Thermochronology

For $^{40}Ar/^{39}Ar$ analysis, concentrates of amphibole, biotite, muscovite, and K-feldspar were separated and handpicked. Mineral separates of unknown age and sanidine from the 27.8 Ma Fish Canyon Tuff (Cebula et al., 1986; Renne et al., 1994) were irradiated for 15–45 h at University of Michigan and McMaster University. Approximately 4–15 mg of material was used for step heating in a double-vacuum furnace, and isotopic compositions of the released gas were measured using a VG 1200 automated mass spectrometer at UCLA. Correction factors for interfering nuclear reactions were determined by using K_2SO_4 and CaF_2 and are listed in the GSA Data Repository (Table DR1).[1] Data were reduced using the in-house data reduction program Agecal, and uncertainties were calculated to the 95% confidence level. Complete isotopic data are found in Table DR1 (see footnote 1).

RESULTS

Kuerti Hanging Wall

Because it is composed mostly of orthogneiss and lacks many aluminosilicate mineral phases, we were unable to make P-T estimates for metamorphic conditions. However, we did collect samples in the Kuerti hanging wall for thermochronological analysis. K-feldspar from sample 6.16.04.4 (see Fig. 2 for location) has a nonuniform release spectrum with a minimum age of 73 Ma and a maximum apparent age of 161 Ma (Fig. 3A).

Sample 6.16.02.3a was collected at ~50 m north of sample 6.16.04.4 (Fig. 2) and exhibits an irregular release spectrum for K-feldspar with an intermediate age maximum at 30% of gas released (Fig. 3B). The release spectra yielded apparent maximum and minimum ages of 194 Ma and 84 Ma, respectively.

Sample 6.15.02.4b was collected ~2 km northeast of the Kuerti thrust from an orthogneiss (Fig. 2). The release spectrum for K-feldspar increases in age monotonically with the exception of the last 20% of gas released, which was likely the result of melting at temperatures above 1200 °C (Fig. 3C). The minimum apparent age of this spectrum is 97 Ma, while its maximum age (before the 1200 °C step) is 230 Ma. The weighted mean age for 57% of the gas released from this sample is 213 ± 1 Ma.

Sample 6.15.02.5a is from a deformed granitic dike that intrudes the host orthogneiss in the Kuerti hanging wall (Fig. 2). Biotite from the dike

yields a release spectrum with an age gradient over the first 30% of gas released. The weighted mean age of 250 ± 2 Ma was calculated for 68% of the gas released (Fig. 3D). K-feldspar from the same sample has a minimum apparent age of 103 Ma and a maximum apparent age of 240 Ma, neglecting the first two steps (0.5% of gas released) and the final steps above 1100 °C (16% of gas released) (Fig. 3E). Sample 6.15.02.5b is from the orthogneiss intruded by the dike and represents the majority of the Kuerti hanging-wall rock type (Fig. 2). The biotite release spectrum from the sample displays a simple plateau, with the exception of an age gradient over the first two steps (7% of gas released). The remainder of the gas (93%) yields a weighted mean plateau age of 262 ± 3 Ma (Fig. 3F).

Barils Hanging Wall

The presence of pelitic bulk compositions allowed us to obtain thermobarometric estimates from the Barils hanging wall (including some samples collected at 6.18.02.6, adjacent to the stretched marble of the Balaerqishi Shear Zone). The four samples analyzed so far are garnet-bearing mica schists. A garnet zoning profile from the most zoned sample, 6.18.92.5c, is shown in Figure 4. The garnets typically display compositionally homogeneous cores, with Fe# increasing (by 1%–4%), X_{Mg} (in mode %) decreasing by <1%–3%, constant to decreasing X_{Ca} (<1%), and X_{Mn} increasing (by 2%–5%) at the rim in three of the four samples. These compositional variations are consistent with diffusional zoning (e.g., Spear, 1993), interpreted to reflect moderately high temperature conditions. In addition, the X_{Mg} and Fe# patterns indicate that retrograde net-transfer reactions may have occurred and potentially led to overestimates of temperatures (e.g., Kohn and Spear, 2000). However, retrieved conditions (5.8 kbar, 615 °C) are broadly compatible with results from other studies in the Altai (Briggs et al., 2007) and expectations based upon the peltic petrogenetic grid (Spear and Cheney, 1989) and garnet zoning patterns (e.g., Yardley, 1977).

Sample 6.18.02.2 was collected from schist with garnet, muscovite, biotite, and plagioclase with an average composition of An_{36} (Table 1). This sample preserved some growth zoning in its garnets, including a decrease in Mn from core to rim and only a minor increase in Fe/(Fe + Mg) at the rim. Retrieved P-T conditions are 5.8 ± 1.7 kbar and 643 ± 141 °C (Fig. 5).

Sample 6.18.02.5c was collected from schist that contains garnet, biotite, muscovite, and plagioclase with an average composition of An_{11} (Table 1). The garnets exhibit diffusional zoning and yield P-T estimates of 5.3 ± 1.9 kbar and 565 ± 117 °C (Fig. 5).

Samples 6.18.02.6f and 6.18.02.6e, both staurolite-bearing mica schists, have garnets which are the most homogenous, but have recognizable increases of Mn and Fe# at the rims consistent with diffusional zoning. In 6.18.02.6e, staurolite forms large (reaching centimeters in length) poikioblasts. P-T conditions of 5.0 ± 1.8 kbar and 590 ± 40 °C were obtained for 6.18.02.6f, while sample 6.18.02.6e resulted in 7.0 ± 2.0 kbar and 664 ± 70 °C (Fig. 5). The P-T estimates from these two samples at the same location overlap somewhat, consistent with the staurolite + biotite assemblage (Spear and Cheney, 1989).

Average P-T conditions for the Barils hanging wall (~5.75 kbar, 615 °C) are shown with a dark gray filled ellipse and solid dot in Figure 5. With a goal of determining the age of this metamorphism, we conducted in situ Th/Pb ion-microprobe dating of monazite from sample 6.18.02.6 g (see Fig. 2 for location). Nine monazite inclusions in garnet yield ages from 222 ± 13 Ma to 288 ± 12 Ma (Table 2), with a dominant peak at ca. 231 Ma (Fig. 6). In some cases, textural relationships indicate that monazite grains with older ages are located closer to the apparent center of the including garnet, but this is not consistent for all monazite examined. The entire age distribution yields a weighted mean age of 246 ± 18 Ma (mean square of weighted deviate [MSWD] 3.8). However, the shape of the probability distribution function (Fig. 6) indicates two age populations may exist—a small, Early Permian (ca. 275–280 Ma) one as well as the Triassic population (ca. 230 Ma).

The $^{40}Ar/^{39}Ar$ thermochronological analyses of four samples reveal information about the exhumation history of the Barils hanging wall (Fig. 7). In general, muscovite and biotite release spectra show some degree of age gradients over the first 4%–18% of gas released. Muscovite weighted mean ages range from ca. 230 to 209 Ma, while the biotite ages range from 204 to 179 Ma.

Tuehongshat-Erqishi Shear Zone

Sample 6.15.02.6 was collected from a sheared granitoid dike in the left-slip Tuehongshat-Erqishi shear zone (Fig. 2) and yields a weighted mean $^{206}Pb/^{238}U$ age of 258 ± 11 Ma from ten concordant zircon analyses (Briggs, 2007). The shear zone initiated sometime after this date in the Late Paleozoic. K-feldspar from the sample yields a concave-upward release spectrum, with a maximum apparent age of 223 Ma and a minimum apparent age of 93 Ma (Fig. 3G).

East Side of the Fuyun Fault

All the samples discussed above were collected west of the Fuyun fault. In order to have some data about the geologic history of the
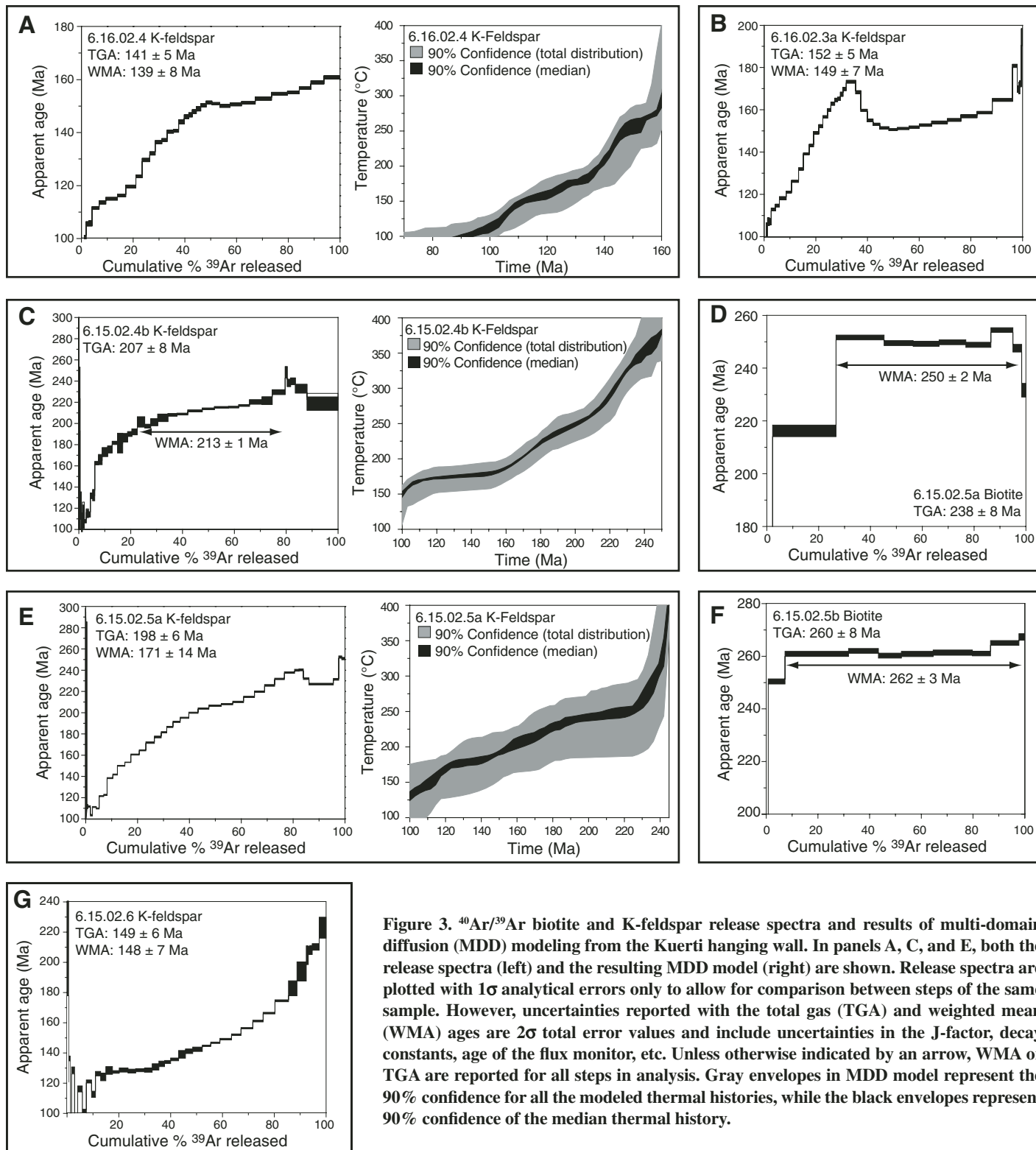
Figure 3. ⁴⁰Ar/³⁹Ar biotite and K-feldspar release spectra and results of multi-domain diffusion (MDD) modeling from the Kuerti hanging wall. In panels A, C, and E, both the release spectra (left) and the resulting MDD model (right) are shown. Release spectra are plotted with 1σ analytical errors only to allow for comparison between steps of the same sample. However, uncertainties reported with the total gas (TGA) and weighted mean (WMA) ages are 2σ total error values and include uncertainties in the J-factor, decay constants, age of the flux monitor, etc. Unless otherwise indicated by an arrow, WMA or TGA are reported for all steps in analysis. Gray envelopes in MDD model represent the 90% confidence for all the modeled thermal histories, while the black envelopes represent 90% confidence of the median thermal history.
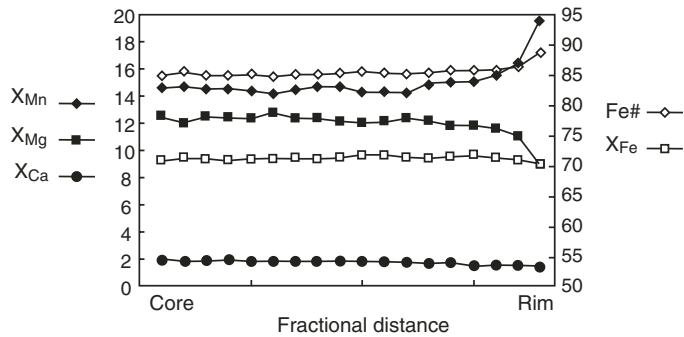
Figure 4. Zoning line from a garnet in a metapelite sample 6.18.02.5c in the Barils hanging wall. Compositional parameters in mole%. X_{Mn}, X_{Mg}, and Fe# show up to 5% variations in the outer 25 μm of the garnet grain. This zoning is compatible with diffusional or retrograde zoning during heating and decompression.
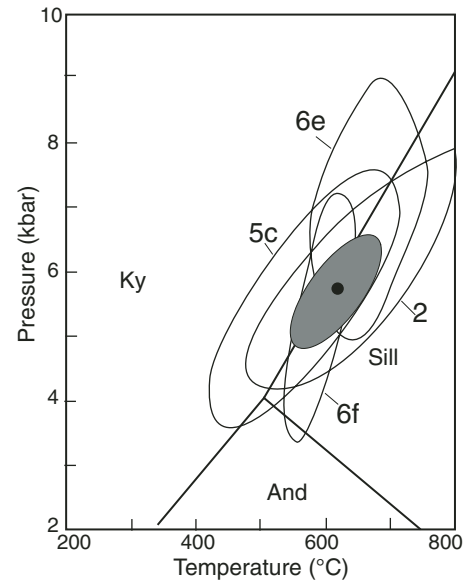

Figure 5. P-T (pressure-temperature) results from Barils hanging wall. Each unfilled error ellipse is the P-T result from a single sample (2σ). The average of the four samples for the Barils hanging wall is shown by charcoal-gray filled error ellipse (1σ) with a black solid dot in the center at P = 5.75 kbar and T = 615 °C. Sample numbers were abbreviated as follows: 2—6.18.02.2; 5c—6.18.02.5c; 6e—6.18.02.6e; and 6f—6.18.02.6f. Aluminosilicate triple junction shown for reference: Ky—kyanite, Sill—sillimanite, And—andalusite.

eastern part of the study area, we analyzed two biotite samples for $^{40}Ar/^{39}Ar$ thermochronology (Fig. 2). Sample 6.15.02.8a from a schist unit has a release spectrum that displays an age gradient for the first 25% of gas released, rising to a plateau at ca. 200 Ma (Fig. 8B). Sample 6.15.02.9 is from a deformed granite that has a U-Pb zircon age of 409 ± 7 Ma (Wang et al., 2006); its biotite yields a release spectrum with a plateau-like segment with a weighted mean age of 156 ± 3 Ma (Fig. 8A). Again, the age gradient in the release spectra for both of these samples implies slow cooling, which may explain the ~35 Ma difference in biotite cooling ages for two samples located so near one another.

DISCUSSION

Temperature-Time Paths and Deformation across the Chinese Altai

In the northern Chinese Altai, schists yield information regarding the medium- to high-temperature history of the Barils hanging wall. The uncertainties on P-T results from individual samples yield a range of possible metamorphic temperature conditions, from as low as 565 ± 117 (~450 °C) to as high as 643 ± 117 (~780 °C). However, our weighted average conditions from four samples of ~615 °C and 5.75 kbar are compatible with petrologic observations, such as diffusional garnet zoning and the existence of staurolite + biotite, which requires a minimum of ~550 °C (Spear and Cheney, 1989). Accurately demonstrating the timing of these conditions is complicated by the fact that monazite can grow in conditions as low as greenschist facies (~400 °C, Townsend et al., 2000) to as high as upper amphibolite to granulite facies (>700 °C, Pyle and Spear, 2003) via many different reactions (e.g., Catlos et al., 2002). Studies

have shown that the chemical composition and zoning of monazite, as well as a detailed analysis of petrologic indicators of monazite-forming reactions can greatly aid in interpreting ages (Pyle and Spear, 2003; Kohn and Malloy, 2004; Kohn et al., 2005). Given the reconnaissance nature of this study, we rely upon the simple interpretation that garnet-hosted inclusions were included during garnet-grade metamorphism (e.g., Catlos et al., 2002) and interpret the ages as being linked to the high-T (~615 °C) metamorphism recorded in these rocks. Furthermore, the P-T conditions from the same location as our monazite sample (samples 6.18.02. 6e, 6f, and 6g) are based upon the staurolite-bearing assemblage there, and work has demonstrated monazite growth as a result of staurolite-in reactions in pelitic rocks (Kohn and Malloy, 2004)

The monazite ages from individual analyses span 66 Ma. All monazites analyzed were included within garnets, and spatial relationships (location within the grain or adjacent to cracks or other inclusions) do not have a consistent age correlation. The preservation of multiple monazite growth events, even within a single grain, is common in metamorphic rocks (e.g., Pyle and Spear, 2003; Kohn et al., 2005) and the asym-

metric, two-humped probability distribution function for the distribution may indicate that two separate age populations exist. Furthermore, the smaller population of Early Permian monazites (ca. 280 Ma) is the same age as monazite analyzed from the Ertix hanging wall to the south (Briggs et al., 2007). However, given the small number of analyses, the most straightforward interpretation of the data is that the weighted mean of the entire population

TABLE 2. MONAZITE ISOTOPIC DATA FOR ALTAI METAPELITE

Mount-grain-spot	$^{208}Pb*/^{232}Th$	Standard error	Th/U	$^{208}Pb*$ (%)	ThO_2/Th	$^{208}Pb/^{232}Th$ age (±1σ)
Barils metapelitic schist (6.18.02.6g)						
m1-4-4	0.01104	6.57E-04	20.51	78.5	3.623	222.0 ± 13.1
m1-7-1	0.01120	5.92E-04	26.7	91.3	2.431	225.1 ± 11.8
m1-4-1	0.01135	7.23E-04	18.83	58.9	2.538	228.2 ± 14.4
m1-5-1	0.01146	6.41E-04	13.97	87.1	3.604	230.4 ± 12.8
m3-a-1	0.01171	5.49E-04	12.33	96.0	2.652	235.4 ± 11.0
m3-c-7	0.01248	5.97E-04	10.52	85.0	2.793	250.7 ± 11.9
m1-4-2	0.01314	8.18E-04	15.8	64.8	3.281	263.9 ± 16.3
m3-d-12	0.01371	6.15E-04	11.49	98.0	2.747	275.3 ± 12.3
m3-c-9	0.01434	6.23E-04	8.769	88.1	3.097	287.8 ± 12.4
						Weighted mean $^{208}Pb/^{232}Th$ age (2σ) 246 ± 18 Ma.

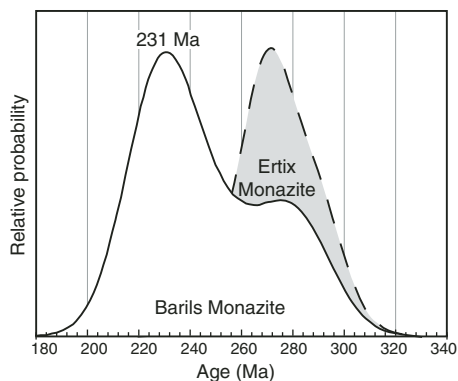*Note:* mean square of weighted deviates (MSWD) = 3.6.

Figure 6. Probability distribution function for monazite from the Barils hanging wall (in white). Gray shaded peak is the probability distribution for monazite ages from the Ertix hanging wall (from Briggs et al., 2007).

represents the best estimate of the age of a single growth event. Hence, the Barils hanging wall was experiencing conditions of 610 ± 35 °C and 5.7 ± 1.8 kbar at 246 ± 18 Ma (Fig. 9).

Cooling after the Triassic metamorphic conditions described above is recorded via mica ages for the Barils hanging wall. Muscovite release spectra indicate cooling through the muscovite closure temperature occurred in the Middle to Late Triassic (209–230 Ma). The biotite closure temperature was reached shortly thereafter (between ca. 204 and 179 Ma) in the Latest Triassic to Early Jurassic. Unfortunately, no information is available for lower-temperature portions of the cooling history for the Barils hanging wall, aside from sparse Cretaceous fission-track ages

(Yuan et al., 2006). The considerable gap in ages and temperatures makes the form of the thermal history difficult to assess.

To the south, the Kuerti hanging-wall biotite ages are 250 and 262 Ma (Late Permian to Early Triassic), and spectra exhibit age gradients that could be interpreted to reflect slow cooling through a biotite closure temperature (e.g., Robinson et al., 2004). Maximum apparent ages from K-feldspar release spectra vary from 240 Ma far from the fault, to as young as 161 Ma adjacent to the fault. The oldest maximum argon ages (ca. 240 Ma seen in 6.15.02.5a) are consistent with slow cooling through a K-feldspar closure temperature following the cooling through biotite closure (at ca. 250–260 Ma). In addition, all of the K-feldspar spectra show some degree of argon loss, and the youngest maximum apparent ages are recorded closest to the mapped trace of the fault (samples 6.16.02.4 and 6.16.02.3a).

The properties of K-feldspar were further exploited when applying multi-domain diffusion (MDD) modeling (Lovera et al., 1997) to three samples in the Kuerti hanging wall. Readers are referred to McDougall and Harrison (1999) and Parsons et al. (1999) for discussions of the application and caveats associated with this method. The sample farthest from the Kuerti thrust, 6.15.02.5a, indicates the fastest cooling of its cooling history (~7 °C/Ma) occurred before ca. 225 Ma. However, in the absence of additional information about the thermal history of these rocks above ~300 °C, this phase of relatively fast cooling may be erroneous. The remainder of the cooling history indicates fairly uniform cooling rates into the Cretaceous. We

made the use of isothermal duplicates to correct for minimal Cl-derived excess [40]Ar (Harrison et al., 1994) for the first 3% of gas released for sample 6.15.02.4b. The MDD–modeled thermal history appears to have two stages: moderate cooling at a rate of ~2.5 °C/Ma between 240 and 160 Ma and nearly isothermal conditions between 160 and 110 Ma (Fig. 3C). Nearer the thrust, the "humped" release spectrum of 6.16.02.3a prevented successful MDD modeling, while 6.16.02.4 records the bulk of cooling between 160 and 100 Ma. This is again in sharp contrast to the K-feldspar results farther north of the fault, which record slow cooling to isothermal conditions during this Late Jurassic to Early Cretaceous time period. These Kuerti hanging-wall results indicate that the rocks were exhumed from depth through biotite and K-feldspar bulk-closure temperatures between ca. 262 Ma and ca. 230 Ma, respectively.

It is informative to compare our results with those of Briggs et al. (2007) for the Ertix thrust in the south. In situ Th/Pb dates of four included monazites in synkinematic garnet and six monazites from matrix of schists from the Ertix hanging wall have a weighted mean age of 278 ± 9 Ma (Fig. 6; Briggs et al., 2007). Muscovite, biotite, and K-feldspar cooling ages are ca. 275 Ma, 257–265 Ma, and 269–265 Ma, respectively (Briggs et al., 2007). While the biotite spectra were disturbed, the shape of muscovite and K-feldspar release spectra and the similarity in ages from all three phases indicated rapid cooling (Fig. 9). This rapid cooling was also reflected in the resulting MDD thermal history (Fig. 9). In general, the Ertix hanging wall cooled completely from amphibolites-facies
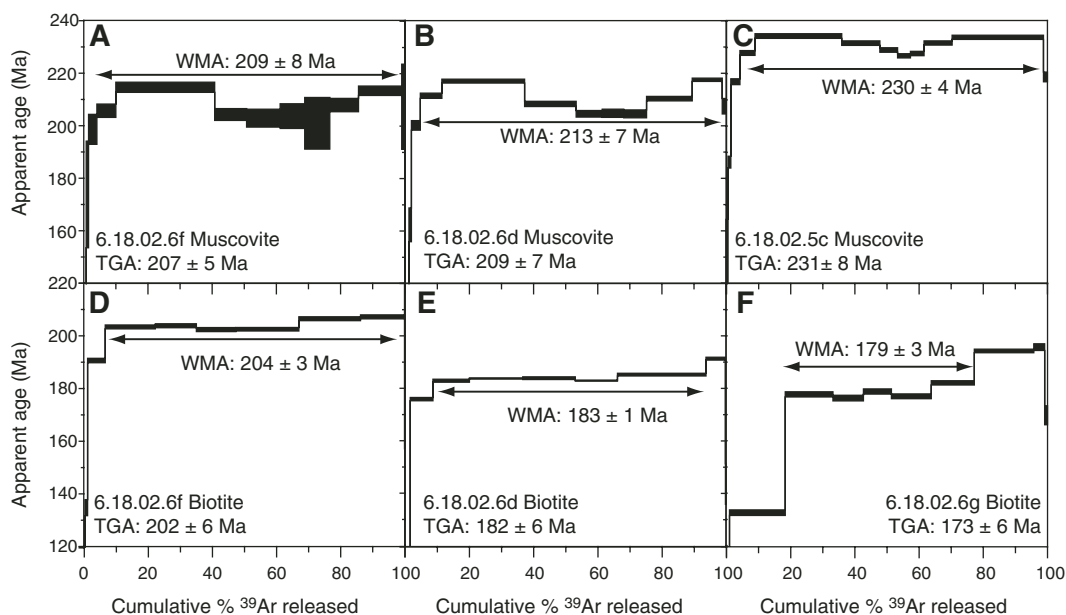

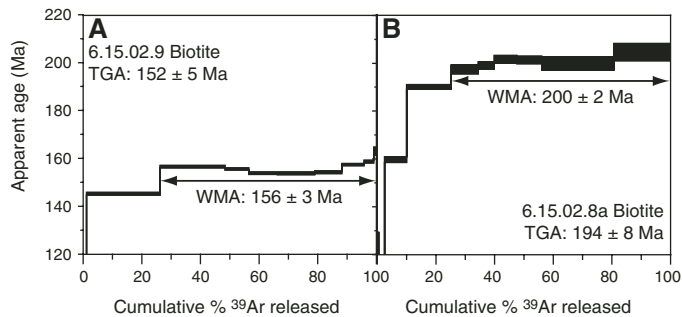**Figure 7. Muscovite and biotite [40]Ar/[39]Ar release spectra from Barils hanging wall.**

Figure 8. Biotite $^{40}Ar/^{39}Ar$ release spectra for samples from the east side of the Fuyun fault.

conditions to ~150 °C within the Permian, and apatite fission-track modeling is consistent with that thermal history (Fig. 9, Yuan et al., 2006).

Timing of Deformation across the Chinese Altai Range

The data presented above indicate three potentially distinct temperature-time paths for the Ertix, Kuerti, and Barils hanging walls (Fig. 9). Slip on the Ertix thrust, coupled with erosion at the Earth's surface, was responsible for the rapid cooling of its hanging wall during the Permian (Briggs et al., 2007). Just to the north, the Kuerti hanging wall records slightly younger mica and K-feldspar argon ages. This Late Permian to Triassic cooling is also interpreted as the result of vertical transport through the crust, via slip on either of the underlying Kuerti or Ertix thrust faults, given that the hanging walls of both faults seem to record similar (250–265 Ma) biotite ages (Briggs et al., 2007). Furthermore, K-feldspar release spectra exhibit progressively younger ages with proximity to the fault. The most disturbed spectra come from samples within <50 m of the fault, which display evidence for brittle deformation at the hand-sample and thin-section scale, such as fractures and undulatory extinction in quartz. Hence, we interpret these observations to indicate that the argon loss event recorded in the ca. 160 Ma K-feldspar maximum apparent age and cooling history from a brittly deformed sample adjacent to the fault is interpreted to reflect a Late Jurassic to Early Cretaceous deformation along the Kuerti thrust. The new P-T data and monazite ages suggest that the Barils hanging wall experienced near-peak metamorphism of 610 ± 35 °C and 5.7 ± 1.8 kbar in the Late Permian to Triassic. Additionally, the Barils hanging wall records biotite ages of 179–204 Ma, indicating cooling through the biotite closure temperature in the Late Triassic to Early Jurassic. We take this thermal history to be fault controlled, and

consider the vertical movement through the crust because of slip on thrusts, coupled with erosion, to be responsible for the moderate cooling recording in the calculated temperature-time paths. A fault-related origin for this cooling history is supported given the contrast between the thermal history for the Barils hanging wall compared to the Ertix hanging wall, for example. Indeed, the bulk of monazite ages for the Barils schist have ages younger than K-feldspar ages for the Ertix hanging wall. Similarly, muscovite and biotite ages from the Barils hanging wall are 40–100 Ma younger than their counterparts in the Ertix hanging wall. Following the assumption that cooling in these rocks is thrust related, and observing the youngest mica ages in the orogen are in the Barils hanging wall, it follows that the Barils fault was active the most recently. However, we have little direct information regarding the timing of most recent fault motion.

U–Pb zircon dating of a granitoid in the Tuhongshat-Erqishi shear zone requires its motion to have occurred after 258 ± 11 Ma. Because K-feldspar from this location and nearby indicates that these rocks were at temperatures of <150 °C since 150 Ma, and because the ductile deformation this sample experienced likely occurred at temperatures above 300 °C, we estimate that this shear zone was active between the latest Permian and the Late Jurassic. Therefore, left-lateral deformation occurred during or after the Permo-Triassic contraction in the Altai Range (Fig. 10). Additionally, this shear zone does not manifest itself as the orogen-scale structure envisioned in some of the tectonic models for the region. This structure's modest extent contributes to our interpretation that the strike-slip structures are less significant in accommodating strain relative to the thrusts in the region.

From the available data and comparison of cooling histories (Figs. 9 and 10), we make the following interpretations for the timing of motion on the three major thrusts across the southern Chinese Altai Range: (1) the Ertix thrust was

active after metamorphism recorded as early as ca. 293 Ma, and its hanging wall was cooled to shallow crust temperatures after ca. 245 Ma (see Briggs et al., 2007); (2) the Kuerti fault had two episodes of motion, one at 245–220 Ma immediately after the terminal motion on the Ertix thrust, and the other with a maximum age of ca. 160 Ma; (3) the Barils thrust was active sometime after the metamorphic growth of monazite at 246 ± 18 Ma; and (4) localized left-slip shear deformation occurred sometime after 258 Ma and before 150 Ma (Fig. 10).

The above fault chronology suggests the Permian–Jurassic Altai thrust belt to have formed by out-of-sequence thrusting and, at least demonstrably, that the Kuerti was active more recently than the Ertix. The geochronologically supported interpretation that the Kuerti thrust postdates the Ertix fault is consistent with the field relationship shown in Figure 2. As discussed above, the Kuerti fault truncates folds and the Dahantir thrust in the Ertix hanging wall. Because these folds and the Dahantir are parallel to the Ertix fault, it is likely they formed synchronously with the Ertix fault, and would provide further evidence that the Kuerti postdates the Ertix. However, the presence of the Cenozoic Fuyun fault obscures this critical relationship, and more detailed fieldwork is required to establish the direct crosscutting relationship between the Ertix fault and the Kuerti thrust.

Model Testing and Regional Implications

The timing and style of deformation determined from this study help test the existing tectonic models for the development of the Chinese Altai Range. Because arc magmatism in the region occurred between 470 Ma and 285 Ma (Han et al., 1997; Chen and Jahn, 2002; Windley et al., 2002; Wang et al., 2006; Briggs et al., 2007), the Permian to Jurassic deformation mostly postdates the arc magmatism. The slight overlap of arc magmatism and initial deformation across the Altai Range could be an artifact of the age uncertainties or a result of continuing arc-like magmatism after the closure of the Junggar basin at or before the end of the Early Permian (ca. 256 Ma) when the Altai region recorded its last marine sedimentation (e.g., Carroll et al., 1990; Allen et al., 1995).

As mentioned above, the single-arc model of Şengör et al. (1993) requires synsubduction strike-slip faulting to duplicate progressively the originally >6000-km-long arc in map view, thereby expanding the orogen. This model specifically predicts the Ertix fault to be active between ca. 520 and 340 Ma with >1600-km motion during the development of the magmatic arc (Fig. 10). For a fault with such a large
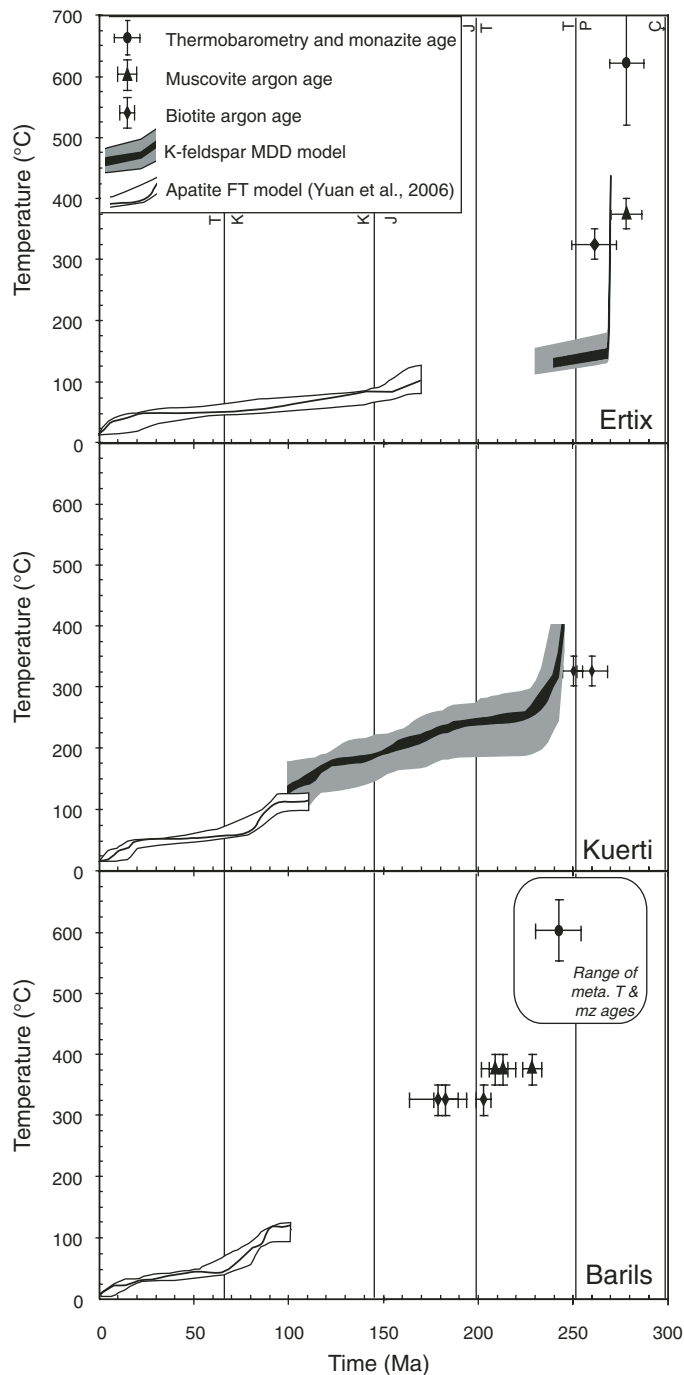
Figure 9. Temperature-time summaries of data from Ertix (top panel), Kuerti (middle panel), and Barils (bottom panel) hanging walls, from this study, Yuan et al. (2004), and Briggs et al. (2007). In the Barils panel, the rounded rectangle shows the full range of ages from individual monazite analyses and retrieved metamorphic temperatures. The average monazite age and metamorphic temperature with standard errors are shown with the ellipse and error bars; the argon ages are paired with assumed closure temperatures (triangles and diamonds). Boundaries between time periods are shown for reference (International Commission on Stratigraphy). Abbreviations: FT—fission track; meta.—metamorphic; MDD— multi-domain diffusion; mz—monazite; T—temperature.

magnitude and longevity of motion, it would require a broad right-lateral, strike-slip deformation zone several hundreds of kilometers wide, similar to the San Andreas Fault system (Powell, 1993). As shown by Briggs et al. (2007) and this study, the major structures across the Chinese Altai Range are thrusts and left-slip shear zones rather than right-lateral, synsubduction faults as required by the model of Şengör et al. (1993). In addition, these structures were likely active in the Permo-Triassic and Jurassic, significantly younger than the predicted fault motion and postdating most of the arc magmatism (Fig. 10).

Badarch et al. (2002) and Xiao et al. (2004) envisioned that the Altai Range was occupied by a long-lived arc starting in the Cambrian with the arc axis located in the northeast of the range (present orientation) and migrates to the present Altai Range in the Devonian. In contrast, Wang et al. (2006) suggest that the main tectonic event in the Altai Range is the closure of a backarc basin after 375 Ma in the Late Devonian (Fig. 10). Although Wang et al. (2006) clearly demonstrated ductile deformation during emplacement of plutons with ages ranging from 460 to 370 Ma, they did not identify any Late Devonian major faults whose motion could be correlated with the inferred backarc-basin collapse. The main evidence for the presence of a backarc basin by Wang et al. (2006) is the occurrence of a Late Devonian–Early Carboniferous mafic igneous complex in the Kuerti hanging wall, which was interpreted to represent an oceanic crust in a backarc setting (Xu et al., 2002). This mafic complex and its associated radiolarian chert were interpreted by Wang et al. (2006) as ophiolitic fragments marking the site of backarc-basin closure. Because the mafic complex is in tectonic contact with its surrounding rocks, dominantly gneisses and migmatite (Xu et al., 2002) that are together bounded by the post-arc Permo-Triassic faults (i.e., the Kuerti fault in the south and the Barils fault to the north), reconstructing the paleo–plate-tectonic setting requires restoring deformation across the younger Permo-Triassic thrusts. We concur with the proposal of Briggs et al. (2007) that the Ertix thrust developed within an accretionary complex and brought up the deeply buried mélange materials over their originally overlying shallow crustal Devonian arc. The duplication of the mélange complex, which also consists of mafic components, by the Ertix fault produces the appearance that multiple sutures exist across the Altai Range and its foothills directly to the south. We suggest that similar duplication also occurred along the Kuerti fault, bringing up deeply buried oceanic fragments to the surface. A consequence of this tectonic process is the apparent exposure of multiple sutures or mélange zones, leading to the erroneous conclusions that
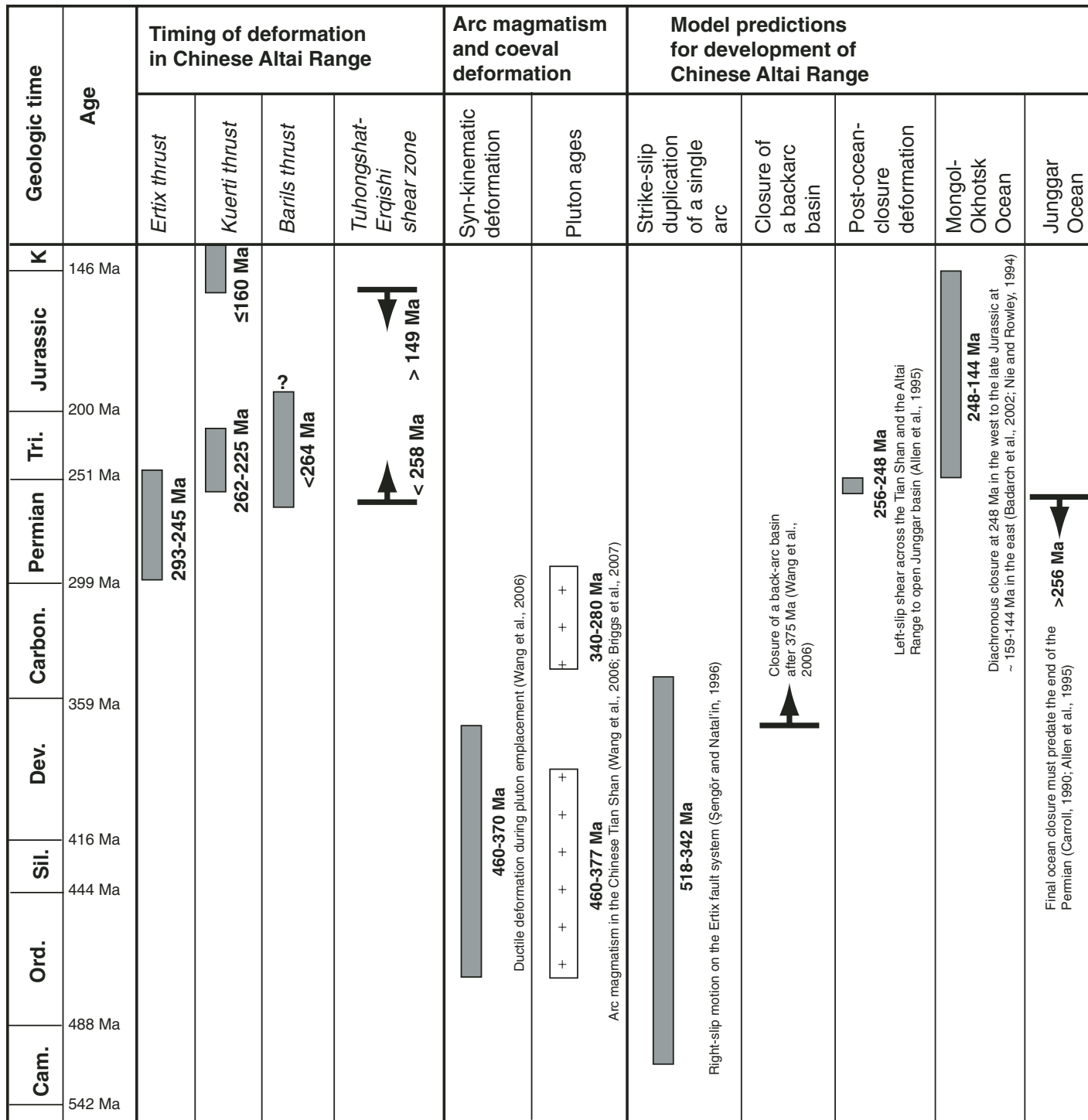
Figure 10. A summary of fault chronology in the context of regional arc magmatism and predictions of tectonic models for the development of the Chinese Altai Range.

The figure plots the following against a geologic time axis (Cam. 542 Ma through K 146 Ma):

Timing of deformation in Chinese Altai Range				Arc magmatism and coeval deformation		Model predictions for development of Chinese Altai Range				
Ertix thrust	*Kuerti thrust*	*Barils thrust*	*Tuhongshat-Erqishi shear zone*	Syn-kinematic deformation	Pluton ages	Strike-slip duplication of a single arc	Closure of a backarc basin	Post-ocean-closure deformation	Mongol-Okhotsk Ocean	Junggar Ocean
293–245 Ma	≤160 Ma; 262–225 Ma	? ; <264 Ma	>149 Ma ; <258 Ma	460–370 Ma — Ductile deformation during pluton emplacement (Wang et al., 2006)	340–280 Ma; 460–377 Ma — Arc magmatism in the Chinese Tian Shan (Wang et al., 2006; Briggs et al., 2007)	518–342 Ma — Right-slip motion on the Ertix fault system (Şengör and Natal'in, 1996)	Closure of a back-arc basin after 375 Ma (Wang et al., 2006)	256–248 Ma — Left-slip shear across the Tian Shan and the Altai Range to open Junggar basin (Allen et al., 1995)	248–144 Ma — Diachronous closure at 248 Ma in the west to the late Jurassic at ~ 159–144 Ma in the east (Badarch et al., 2002; Nie and Rowley, 1994)	>256 Ma — Final ocean closure must predate the end of the Permian (Carroll, 1990; Allen et al., 1995)

multiple arcs were present in the region (also see Kapp et al., 2003 for a similar geologic setting in western Tibet).

Our inferred timing of left-slip transpressional tectonics in the Chinese Altai Range could be consistent with the model of Allen et al. (1995) that opening of the Junggar basin was caused by a pull-apart mechanism between two left-slip systems in the Altai Range and the Tian Shan. The next test for the model is to examine the existence of linking normal faults connecting the two left-lateral fault zones.

Late Jurassic contraction followed by Early Cretaceous extension has been long known along the northern margin of the North China craton and southern Mongolia (Davis et al., 1996, 2002; Webb et al., 1999; Dumitru and Hendrix, 2001; Graham et al., 2001; Johnson

et al., 2001; Sjostrom et al., 2001). Our finding of Late Jurassic thrusting in the Chinese Altai Range is the first report of such structures in the region. We note a similar Late Jurassic cooling event (180–150 Ma) in the Russian Altai Range (De Grave and Van den haute, 2002; De Grave et al., 2007) and tentatively suggest that it resulted from the same contractional event.

The cause of Late Jurassic contraction in the North China craton, southern Mongolia, and the Altai Range is not clear. Yin and Nie (1996) and Davis et al. (1996, 2002) have attributed it to the closure of the Mongol-Okhotsk Ocean, which was closed prodiachronously from west to east from the Triassic to the Late Jurassic (Nie and Rowley, 1994; Badarch et al., 2002). In contrast, Dumitru and Hendrix (2001) related the contractional event to collision of the Lhasa terrane against the southern margin of Asia in the present central Tibetan Plateau.

CONCLUSIONS

The southern Chinese Altai Range is dominated by a south-directed thrust belt, which was active from the Permian to the Jurassic and may have accommodated up to tens of kilometers of shortening. The contractional event was potentially coeval with left-slip shear across the range after 258 Ma. Both contractional and left-slip deformation postdate the arc magmatism in the region between 470 and 285 Ma. Detailed geochronologic analysis reveals that out-of-sequence thrusting was a major deformation process during the development of the Altai thrust belt. The Permo-Triassic deformation in this belt is consistent with convergence during the final closure of the Junggar basin. However, the timing of deformation and kinematics of major thrusts are inconsistent with the proposal that the Chinese Altai Range was the locus of long-lived right-slip faulting during oceanic subduction between 520 Ma and 340 Ma. The development of the Permo-Triassic thrust belt exhumed deeply buried rocks (>15 km) to shallow crustal levels. The Permo-Triassic Altai thrust belt was reactivated locally by contraction in the Late Jurassic after 160 Ma. This younger event may result from the final closure of the Mongol-Okhotsk Ocean to the north or the collision of the Lhasa block onto the southern Asian margin in Tibet to the south, both of which occurred in the Late Jurassic.

ACKNOWLEDGMENTS

REFERENCES CITED

Allen, M.B., and Vincent, S.J., 1997, Fault reactivation in the Junggar region, northwest China: The role of basement structures during Mesozoic-Cenozoic compression: The Geological Society of London, v. 154, p. 151–155, doi: 10.1144/gsjgs.154.1.0151.

Allen, M.B., Şengör, A.M.C., and Natalin, B.A., 1995, Junggar, Turfan and Alakol Basins as Late Permian to Early Triassic extensional structures in a sinistral shear zone in the Altaid orogenic collage, Central Asia: The Geological Society of London, v. 152, p. 327–338, doi: 10.1144/gsjgs.152.2.0327.

Badarch, G., Cunningham, D., and Windley, B.F., 2002, A new terrane subdivision for Mongolia: Implications for the Phanerozoic crustal growth of Central Asia: Journal of Asian Earth Sciences, v. 21, no. 1, p. 87–110, doi: 10.1016/S1367-9120(02)00017-2.

Baljinnyam, I., Bayasgalan, A., Borisov, B.A., Cisternas, A., Dem'yanovich, M.G., Ganbaatar, L., Kochetkov, V.M., Kurushin, R.A., Molnar, P., Philip, H., and Vashchilov, Yu.Ya., 1993, Ruptures of major earthquakes and active deformation in Mongolia and its surroundings: Geological Society of America Memoir 181, 62 p.

Briggs, S.M., 2007, Structural, U-Th-Pb geochronologic, thermochronologic, thermobarometric, and geochemical studies of the Chinese Altai Ranges: Implications for the Phanerozoic evolution of the Central Asia Orogenic System: Los Angeles, University of California.

Briggs, S.M., Yin, A., Manning, C.E., Grove, M., Chen, Z.L., and Wang, X.F., 2007, Late Paleozoic tectonic history of the Ertix Fault in the Chinese Altai Mountains and its implications for the development of the Central Asian Orogenic System: Geological Society of America Bulletin, v. 119, p. 944–960, doi: 10.1130/B26044.1.

Buslov, M.M., Watanabe, T., Fujiwara, Y., Iwata, K., Smirnova, L.V., Safonova, I.Y., Semakov, N.N., and Kiryanova, A.P., 2004, Late Paleozoic faults of the Altai region, Central Asia: Tectonic pattern and model of formation: Journal of Asian Earth Sciences, v. 23, no. 5, p. 655–671, doi: 10.1016/S1367-9120(03)00131-7.

Carroll, A.R., Liang, Y., Graham, S.A., Xiao, X., Hendrix, M.S., Chu, J. McKnight, C.L., 1990, Junggar basin, northwest China: trapped Late Paleozoic ocean: Tectonophysics, v. 181, p. 1–14.

Catlos, E.J., Gilley, L.D., and Harrison, T.M., 2002, Interpretation of monazite ages obtained via in situ analysis: Chemical Geology, v. 188, p. 193–215, doi: 10.1016/S0009-2541(02)00099-2.

Cebula, G.T., Kunk, M.J., Mehnert, H.H., Naeser, C.W., Obradovich, J.D., and Sutter, J.F., 1986, The Fish Canyon Tuff: A potential standard for the ^{40}Ar-^{39}Ar and fission-track dating methods: Terra Cognita, v. 6, p. 139–140.

Chen, B., and Jahn, B.M., 2002, Geochemical and isotopic studies of the sedimentary and granitic rocks of the Altai orogen of northwest China and their tectonic implications: Geological Magazine, v. 139, p. 1–13, doi: 10.1017/S0016756801006100.

Cunningham, D., 2005, Active intracontinental transpressional mountain building in the Mongolia Altai: Defining a new class of orogen: Earth and Planetary Science Letters, v. 240, p. 436–444.

Cunningham, W.D., Windley, B.F., Dorjnamjaa, D., Badamgarov, G., and Saandar, M., 1996a, A structural transect across the Mongolian Western Altai: Active transpressional mountain building in central Asia: Tectonics, v. 15, p. 142–156, doi: 10.1029/95TC02354.

Cunningham, W.D., Windley, B.F., Dorjnamjaa, D., Badamgarov, G., and Saandar, M., 1996b, Late Cenozoic transpression in southwestern Mongolia and the Gobi Altai-Tien Shan connection: Earth and Planetary Sciences, v. 140, no. 1–4, p. 67–82.

Cunningham, W.D., 1998, Lithospheric controls on Late Cenozoic construction of the Mongolian Altai: Tectonics, v. 17, p. 891–902, doi: 10.1029/1998TC900001.

Cunningham, W.D., 2001, Cenozoic normal faulting and regional doming in the southern Hangay region, Central Mongolia: Implications for the origin of the Baikal Rift Province: Tectonophysics, v. 331, no. 4, p. 389–411.

Davis, G.A., Qian, X., Zheng, Y., Yu, H., Wang, C., Tong, H.M., Gehrels, G.E., Shafiquallah, M., and Fryxell, J.E., 1996, Mesozoic deformation and plutonism in the Yunmeng Shan: A Chinese metamorphic core complex north of Beijing, *in* Yin, A. and Harrison, T.M., eds., The tectonic evolution of Asia: Cambridge, Cambridge University Press, p. 253–280.

Davis, G.A., Darby, B.J., Zheng, Y., and Spell, T.L., 2002, Geometric and temporal evolution of an extensional detachment fault, Hohhot metamorphic core complex, Inner Mongolia, China: Geology, v. 30, p. 1003–1006, doi: 10.1130/0091-7613(2002)030<1003:GATEOA>2.0.CO;2.

De Grave, J., and Van den haute, P., 2002, Denudation and cooling of the Lake Teletskoye Region in the Altai Mountains (South Siberia) as revealed by apatite fission-track thermochronology: Tectonophyics, v. 349, p. 145–159, doi: 10.1016/S0040-1951(02)00051-3.

De Grave, J., Buslov, M.M., Van den haute, P., 2007, Distant effects of India-Eurasia convergence and Mesozoic intracontinental deformation in Central Asia: Constraints from apatite fission-track thermochronology: Journal of Asian Earth Sciences, v. 29, p. 188–204.

Dobretsov, N.L., Berzin, N., and Buslov, M.M., 1995, Opening and tectonic evolution of the Paleo-Asian Ocean: International Geology Review, v. 37, p. 335–360.

Dumitru, T.A., and Hendrix, M.S., 2001, Fission-track constraints on Jurassic folding and thrusting in southern Mongolia and their relationship to the Beishan thrust belt of northern China: Geological Society of America, v. 194, p. 215–229.

Graham, S.A., Hendrix, M.S., Johnson, C.L., Badamgarav, D., Badarch, G., Amory, J., Porter, M., Barsbold, R., Webb, L.E., and Hacker, B.R., 2001, Sedimentary record and tectonic implications of Mesozoic rifting in southeast Mongolia: Geological Society of America Bulletin, v. 113, p. 1560–1579, doi: 10.1130/0016-7606(2001)113<1560:SRATIO>2.0.CO;2.

Han, B.F., Wang, S.G., Jahn, B.M., Hong, D.W., Kagami, H., and Sun, Y.L., 1997, Depleted-mantle source for the Ulungur River A-type granites from North Xinjian, China: Geochemistry and Nd-Sr isotopic evidence, and implications for Phanerozoic crustal growth: Chemical Geology, v. 138, p. 135–159, doi: 10.1016/S0009-2541(97)00003-X.

Harrison, T.M., Heizler, M.T., and Lovera, O.M., Chen, W., and Grove, M., 1994, A chlorine disinfectant for excess argon released from K-feldspar during step heating: Earth and Planetary Science Letters, v. 123, p. 95–104.

Harrison, T.M., McKeegan, K.D., and Le Fort, P., 1995, Detection of inherited monazite in the Manaslu leucogranite by ^{208}Pb/^{232}Th ion microprobe dating: Crystallization age and tectonic significance: Earth and Planetary Science Letters, v. 133, p. 271–282, doi: 10.1016/0012-821X(95)00091-P.

Harrison, T.M., Grove, M., McKeegan, K.D., Coath, C.D., Lovera, O.M., Le Fort, P., 1999, Origin and episodic emplacement of the Manaslu Intrusive Complex, central Himalaya: Journal of Petrology, v. 40, p. 3–19.

He, G., Han, B.F., Yue, Y., and Wang, J., 1990, Tectonic division and crustal evolution of the Altay Orogenic Belt in China: Geoscience of Xinjiang, v. 2, p. 9–20.

Holland, T., and Powell, R., 1998, An internally consistent thermodynamic dataset for phases of petrological interest: Journal of Metamorphic Geology, v. 16, p. 309, doi: 10.1111/j.1525-1314.1998.00140.x.

Hsü, K.J., and Chen, H., 1999, Geologic atlas of China: An application of the tectonic facies concept to the geology of China: New York, Elsevier, 262 p.

Jahn, B.M., 2004, The Central Asian Orogenic Belt and growth of the continental crust in the Phanerozoic, *in* Malpas, J., Fletcher, C.J.N., Ali, J.R., and Aitchison,

J.C. eds., Aspects of the tectonic evolution of China: The Geological Society of London, p. 73–100.

Johnson, C.L., Webb, L.E., Graham, S.A., Hendrix, M.S., and Badarch, G., 2001, Sedimentary and structural records of Late Mesozoic high-strain extension and strain partitioning, East Gobi basin, southern Mongolia: Geological Society of America Memoir, v. 194, p. 413–433.

Kapp, P., Murphy, M.A., Yin, A., Harrison, T.M., Ding, L., and Guo, J., 2003, Mesozoic and Cenozoic tectonic evolution of the Shiguanhe area of western Tibet: Tectonics, p. 1029, v. 22, doi: 10.1029/2001TC001332.

Kohn, M.J., and Malloy, M.A., 2004, Formation of monazite via prograde metamorphic reactions among common silicates: Implications for age determinations: Geochimica et Cosmochimica Acta, v. 68, p. 101–113, doi: 10.1016/S0016-7037(03)00258-8.

Kohn, M.J., and Spear, F., 2000, Retrograde net transfer reaction insurance for pressure-temperature estimates: Geology, v. 28, p. 1127–1130, doi: 10.1130/0091-7613(2000)28<1127:RNTRIF>2.0.CO;2.

Kohn, M.J., Wieland, M.S., Parkinson, C.D., and Upreti, B.N., 2005, Five generations of monazite in Langtang gneisses: Implications for chronology of the Himalayan metamorphic core: Journal of Metamorphic Geology, v. 23, p. 399–406, doi: 10.1111/j.1525-1314.2005.00584.x.

Lamb, M.A., Hanson, A.D., Graham, S.A., Badarch, G., and Webb, L.E., 1999, Left-lateral sense offset of Upper Proterozoic to Paleozoic features across the Gobi Onon, Tost, and Zuunbayan faults in southern Mongolia and implications for other central Asian faults: Earth and Planetary Science Letters, v. 173, p. 183–194, doi: 10.1016/S0012-821X(99)00227-7.

Laurent-Charvet, S., Charvet, J., Shu, L., Ma, R., and Lu, H., 2002, Palaeozoic late collisional strike-slip deformations in Tianshan and Altay, Eastern Xinjiang, NW China: Terra Nova, v. 14, no. 4, p. 249–256, doi: 10.1046/j.1365-3121.2002.00417.x.

Laurent-Charvet, S., Charvet, J., Monie, P., and Shu, L.S., 2003, Late Paleozoic strike-slip shear zones in eastern central Asia (NW China): New structural and geochronological data: Tectonics, v. 22, no. 2, p. 1009, doi: 10.1029/2001TC901047.

Lin, A., 1994, Glassy pseudotachylyte veins from the Fuyun fault zone, northwest China: Journal of Structural Geology, v. 16, p. 71–83.

Lovera, O.M., Grove, M., Harrison, T.M. and Mahon, K.I., 1997, Systematic analyses of K-feldspar $^{40}Ar/^{39}Ar$ step-heating experiments 1: Significance of activation energy determinations: Geochimica et Cosmochimica Acta, v. 61, p. 3171–3192.

McDougall, I. and Harrison, T.M., 1999, Geochronology and Thermochronology by the $^{40}Ar/^{39}Ar$ Method: New York, Oxford University Press, 269 p.

Mei, H.J., Yang, X.C., Wang, J.D., Yu, X.Y., Liu, T.G., and Bai, Z.H., 1993, Trace element geochemistry of Late Palaeozoic volcanic rocks on the southern side of the Irtysh River and the evolutional history of tectonic setting, in Tu, G.Z., ed., Progress of solid-earth sciences in northern Xinjiang, China: Beijing, Science Press, p. 199–216.

Nie, S., and Rowley, D.B., 1994, Comment on "Paleomagnetic constraints on the geodynamics history of the major blocks of China from the Permian to the Present" by R.J. Enkin et al: Journal of Geophysical Research, v. 99, p. 18,035–18,042, doi: 10.1029/93JB03283.

O'Hara, K.D., Yang, X., Xie, G., and Li, Z., 1997, Regional δ^{18}O gradients and fluid-rock interaction in the Altay accretionary complex, northwest China: Geology, v. 25, no. 5, p. 443–446, doi: 10.1130/0091-7613(1997)025<0443:ROGAFR>2.3.CO;2.

Parsons, I., Brown, W.L., and Smith, J.V., 1999, $^{40}Ar/^{39}Ar$ thermochronology using alkali feldspars: Real thermal history or mathematical mirage of microtexture?: Contributions to Mineralogy and Petrology, v. 136, p. 92–110.

Powell, R.E., 1993, Balanced palinspastic reconstruction of pre-late Cenozoic paleogeology, southern California: Geologic and kinematic constraints on evolution of the San Andreas fault system: Geological Society of America Memoir 178, p. 1–106.

Pyle, J.M., and Spear, F.S., 2003, Four generations of accessory-phase growth in low-pressure migmatites from SW New Hampshire: The American Mineralogist, v. 88, p. 338–351.

Qu, G., and Zhang, J., 1994, Oblique thrust systems in the Altay Orogen, China: Journal of Southeast Asian Earth Sciences, v. 9, p. 277–287, doi: 10.1016/0743-9547(94)90035-3.

Renne, P.R., Deino, A.L., Walter, R.C., Turrin, B.D., Swisher, C.C., Becker, T.A., Curtis, G.H., Sharp, W.D., and Jaouni, A.R., 1994, Intercalibration of astronomical and radioisotopic time: Geology, v. 22, p. 783–786, doi: 10.1130/0091-7613(1994)022<0783:IOAART>2.3.CO;2.

Robinson, A.C., Yin, A., Manning, C.E., Harrison, T.M., Zhang, S.H., Wang, X.F., 2004, Tectonic evolution of the northeastern Pamir: Constraints from the northern portion of the Cenozoic Kongur Shan extensional system, western China: Geological Society of America Bulletin, v. 116, p. 953–973.

Şengör, A.M.C., and Natal'in, B.A., 1996, Paleotectonics of Asia: Fragments of a synthesis, in Yin, A., and Harrison, T.M., eds., The tectonic evolution of Asia: New York, Cambridge University Press, p. 486–640.

Şengör, A.M.C., Natalin, B.A., and Burtman, V.S., 1993, Evolution of the Altaid tectonic collage and Paleozoic crustal growth in Eurasia: Nature, v. 364, no. 6435, p. 299–307, doi: 10.1038/364299a0.

Sjostrom, D.J., Hendrix, M.S., Badamgarav, D., Graham, S.A., and Nelson, B.K., 2001, Sedimentology and provenance of Mesozoic nonmarine strata in western Mongolia: A record of intracontinental deformation: Geological Society of America Memoir 194, p. 361–388.

Spear, F.S., 1993, Metamorphic phase equilibria and pressure-temperature-time paths: Washington D.C., Mineralogical Society of America Monograph, 799 p.

Spear, F.S., and Cheney, J.T., 1989, A petrogenetic grid for politic schists in the system SiO$_2$-Al$_2$O$_3$-FeO-MgO-K$_2$O-H$_2$O: Contributions to Mineralogy and Petrology, v. 101, p. 149–164, doi: 10.1007/BF00375302.

Tapponnier, P., and Molnar, P., 1979, Active faulting and Cenozoic tectonics of the Tian Shan, Mongolia, and Baykal regions: Journal of Geophysical Research, v. 84, p. 3425–3459, doi: 10.1029/JB084iB07p03425.

Townsend, K.J., Miller, C.F., D'Andrea, J.L., Ayers, J.C., Harrison, T.M., and Coath, C.D., 2000, Low temperature replacement of monazite in the Ireteba Granite, southern Nevada: Geochronological implications: Chemical Geology, v. 172, p. 95–112, doi: 10.1016/S0009-2541(00)00238-2.

Travin, A.V., Vladimirov, V.G., and Boven, A., 2001, Implication of $^{40}Ar/^{39}Ar$ data on the tectonothermal evolution of the Irtysh shear zone (Eastern Kazakhstan), in Jahn, B.M., ed., Continental growth in the Phanerozoic: Evidence from Central Asia Abstract Volume, p. 106–107.

Wang, T., Hong, D., Jahn, B.M., Tong, Y., Wang, Y.B., Han, B.F., and Wang, X., 2006, Timing, petrogenesis, and setting of Paleozoic synorogenic intrusions from the Altai Mountains, Northwest China: Implications for the tectonic evolution of an accretionary orogen:

The Journal of Geology, v. 114, p. 735–741, doi: 10.1086/507617.

Wang, Y., Mooney, W.D., Yuan, X., Coleman, R.G., 2003, The crustal structure from the Altai Mountains to the Altyn Tagh fault, northwest China: Journal of Geophysical Research, v. 108, doi: 10.1029/2001JB000552.

Webb, L.E., Graham, S.A., Johnson, C.L., Badarch, G., and Hendrix, M.S., 1999, Occurrence, age, and implications of the Yagan-Onch Hayrhan metamorphic core complex, southern Mongolia: Geology, v. 27, p. 143–146, doi: 10.1130/0091-7613(1999)027<0143:OAAIOT>2.3.CO;2.

Windley, B.F., Kroner, A., Guo, J.H., Qu, G.S., Li, Y.Y., and Zhang, C., 2002, Neoproterozoic to Paleozoic geology of the Altai orogen, NW China: New zircon age data and tectonic evolution: The Journal of Geology, v. 110, no. 6, p. 719–737, doi: 10.1086/342866.

Windley, B.F., Alexeiev, D., Xiao, W.J., Kroner, A., and Badarch, G., 2007, Tectonic models for accretion of the Central Asian Orogenic Belt: The Geological Society of London, v. 164, p. 31–47, doi: 10.1144/0016-76492006-022.

Xiao, W., Windley, B.F., Badarch, G., Sun, S., Li, J., Qin, K., and Wang, Z., 2004, Palaeozoic accretionary and convergent tectonics of the southern Altaids: Implications for the growth of Central Asia: The Geological Society of London, v. 161, no. 3, p. 339–342.

Xinjiang Bureau of Geology and Mineral Resources (BGMR), 1978, Geologic map of the Fuyun area: Unpublished, scale 1:200,000, 1 sheet.

Xinjiang Bureau of Geology and Mineral Resources (BGMR), 1993, Geologic map of the Daqiao Area: Unpublished, scale 1:200,000, 1 sheet.

Xu, J., Castillo, P.R., Chen, F., Niu, H., Yu, X., and Zhen, Z., 2002, of Late Paleozoic mafic igneous rocks from the Kuerti area, Xinjiang, northwest China: Implications for backarc mantle evolution: Chemical Geology, v. 193, p. 137–154, doi: 10.1016/S0009-2541(02)00265-6.

Yang, X., Xie, G., and Li, Z., 1992, Mylonite-migmatite lithogenic series—An important tectono-dynamic rock forming process: Geotectonica et Metallogenia, v. 16, p. 151–159.

Yardley, B.W.D., 1977, An empirical study of diffusion in garnet: American Mineralogist, v. 62, p. 793–800.

Yin, A., and Nie, S., 1996, A Phanerozoic palinspastic reconstruction of China and its neighboring regions, in Yin, A., and Harrison, T.M., eds., The tectonic evolution of China: Cambridge, Cambridge University Press, p. 442–485.

Yuan, W, Carter, A., Dong, J., Bao, Z., An, Y., Guo, Z., 2006, Mesozoic-Tertiary exhumation history of the Altai Mountains, northern Xinjian, China: New constraints from apatite fission track data: Tectonophysics, v. 412, p. 183–193.

Zhang, C., Liu, Y., and Wei, X., 1992, Ductile shear zones and nappe-gliding structure in Altay: Xinjiang: Journal of Chendu College of Geology, v. 19, no. 1, p. 1–7.

Zonenshain, L.P., Kuzmin, M.I., and Natapov, L.M., 1990, Geology of the USSR: A plate-tectonic synthesis: Washington, D.C., American Geophysical Union, 242 p.

Zorin, Y.A., 1999, Geodynamics of the western part of the Mongolia-Okhotsk collisional belt, Trans-Baikal region (Russia) and Mongolia: Tectonophysics, v. 306, p. 33–56, doi: 10.1016/S0040-1951(99)00042-6.